Editors' Suggestion

Stresslet in a dilute suspension of rigid spheres in an Oldroyd-B fluid

Boon Siong Neo [1] and Eric S. G. Shaqfeh [1,2,*]

[1] *Department of Chemical Engineering, Stanford University, Stanford, California 94305, USA*

[2] *Department of Mechanical Engineering, Stanford University, Stanford, California 94305, USA*

(Received 11 December 2023; accepted 20 February 2024; published 15 March 2024)

The stresslet in a dilute suspension of rigid spheres in an Oldroyd-B fluid under imposed shear and uniaxial exentional flow is studied using a combination of analytical and numerical techniques. Previous work has focused on the stresslet contribution to the per-particle viscosity of a suspension. This contribution has been shown to decrease with increasing suspending fluid elasticity in shear and decrease with increasing strain in transient uniaxial extension. By considering the surface tractions in the Newtonian limit, we propose analytical scalings for the three components of the stresslet—pressure, viscous stress, and polymer stress—as functions of the appropriate Weissenberg or Deborah number. We conduct direct numerical simulations of a dilute sphere in viscoelastic fluid flow to compare against analytical scalings and see good agreement for weak elasticity, with increasing deviations as the fluid becomes increasingly elastic. Finally, we discuss the consequences of these trends on the tractions and stresses experienced by the suspended particles.

DOI: 10.1103/PhysRevFluids.9.033301

I. INTRODUCTION

Many industrial and consumer products in areas such as manufacturing, healthcare, and food can be modeled as particle suspensions. Understanding the rheology of particle suspensions can better inform the formulation and application of these products. In particular, understanding the interactions between the suspending fluid and the suspended particles not only gives insights into the bulk rheology of the suspension but also how the suspended particles are affected by the fluid under an imposed flow. The stress exerted on suspended particles in a suspension subjected to an imposed flow can be an important design parameter in certain applications, e.g., the viability of cells suspended in a carrier gel [1,2], or the rupture of artificial capsules containing active substances [3].

Dilute suspensions of non-Brownian, homogenous, rigid spheres are a model system for analyzing suspension rheology. For such a suspension in a Newtonian suspending fluid in both shear and extensional flow, the viscosity increases by an amount proportional to the shear viscosity of the fluid and the volume fraction of the particles in the suspension—the well-known Einstein viscosity. However, when elasticity is introduced into the fluid, the suspension rheology changes noticeably even when the suspending fluid has constant steady-shear viscosity independent of shear rate, i.e., an Oldroyd-B fluid [4].

In flows of such suspensions under shear, the steady shear viscosity was found to increase with increasing elasticity or shear rate of the suspending fluid, analytically [5,6], numerically [7], and experimentally [8,9]. In extensional flows, previous analytical and numerical studies of the transient extensional behavior [10] found that the extensional per-particle viscosity generally increases to a peak value and then decreases, with increasing strain. Increasing fluid elasticity led to higher peaks and subsequently lower values of the per-particle viscosity, which has now also been predicted for the steady-state extensional viscosity [11].

*esgs@stanford.edu

This behavior has previously been explained by calculating the extra stress in the suspension arising from the presence of the particle. This extra stress was decomposed into two contributions: the particle-induced fluid stress (PIFS), which reflects additional stress in the fluid phase due to the new flow field created by the presence of the particle [12], and the stresslet, which reflects the additional stress in the rigid particle domains since the stress-strain relationship in the particles is different from that of the fluid [13]. The PIFS was found to be the major contribution to the shear-thickening and transient strain behavior of such suspensions [7,10–12]. In contrast, the stresslet contribution to the per-particle viscosity was found to consistently decrease in both shear and extensional flows as the Weissenberg number of the flow increases. Thus, the stresslet contribution displays shear-thinning (in shear flow) and strain-softening (in uniaxial extensional flow) behaviors. This shear-thinning stresslet has been described as "shielding" the particle and decreasing local surface tractions [10,12,14,15]. Shear flow simulations where the rigid particle is replaced by a deformable solid show that increasing fluid elasticity decreases particle deformation and increases particle alignment with the flow direction [16], and additional suspending fluid elasticity causes the stresslet to shear-thin faster [17]. These results for deformable particles show tangible effects of any "shielding" associated with a shear-thinning stresslet. However, a detailed investigation of the underlying mechanism of stresslet shear thinning has not previously been explored; for instance, while it was noted that the stresslet can be shear thickening at particle volume fractions $\geqslant 2.5\%$ for suspensions in shear-thinning polymeric fluids [18], it has not been determined if the stresslet could ever display shear thickening in the dilute regime.

In this paper, we explore the mechanism behind the previously reported trends for the stresslet in both shear and extensional flow. Analytical expressions can be derived for the flow field around spherical particles in a macroscopic linear flow for a Newtonian fluid in the Stokes limit. We observe that due to its hyperbolic nature, the polymer constitutive equation can be directly evaluated along streamlines of the flow, specifically those lying on the particle surface, in the limit of the Newtonian flow fields. This is only true in the Newtonian limit, so investigating if the scaling extends for increasingly elastic fluids is interesting. From evaluating these expressions in shear and extensional flow, we explain how the shear rate on the particle surface affects the local polymer stresses and in turn the stresslet.

II. METHODS

A. Governing equations

We investigate a neutrally buoyant, freely suspended sphere of radius a in an incompressible viscoelastic fluid, with either shear or extensional flow applied in the far field. The fluid surrounding the sphere is described mathematically by conservation of momentum and mass, with the equations rescaled in dimensionless form by a careful choice of scale factors. We define the characteristic fluid timescale τ_c to be either $\dot{\gamma}^{-1}$ (inverse shear rate) or $\dot{\epsilon}^{-1}$ (inverse extension rate) in shear or extensional flow respectively. The characteristic viscous stress scale is η_0/τ_c, where η_0 is the zero shear viscosity of the fluid. The characteristic length scale is the radius of the particle, a. With these scalings, we present the following analysis and equations in dimensionless terms. We consider the problem in the Stokes limit such that the Reynolds number $\mathrm{Re} \equiv \frac{\rho a^2}{\eta_0 \tau_c}$ of the flow is negligibly small. Thus we use the dimensionless Stokes equations for an incompressible fluid:

$$\nabla_j \sigma_{ij}^{\mathrm{total},f} = 0, \tag{1}$$

$$\nabla_i u_i = 0, \tag{2}$$

where u_i is the velocity field in the fluid made dimensionless by a/τ_c and $\sigma_{ij}^{\mathrm{total}}$ is the Cauchy or total stress made dimensionless by η_0/τ_c.

To incorporate viscoelasticity, we assume the total fluid stress $\sigma_{ij}^{\text{total},f}$ arises from the sum of a Newtonian and polymeric contribution:

$$\sigma_{ij}^{\text{total},f} = -p\delta_{ij} + +2\beta E_{ij} + \sigma_{ij}^{\text{poly}}, \tag{3}$$

$$E_{ij} = \frac{1}{2}(\nabla_j u_i + \nabla_i u_j), \tag{4}$$

where p is the (solvent) pressure made dimensionless by η_0/τ_c; σ_{ij}^{p} is the stress arising from polymer molecules in the fluid, also made dimensionless by η_0/τ_c; and $\beta \equiv \frac{\eta_s}{\eta_s+\eta_p}$ is the solvent viscosity over the zero-shear viscosity. To describe the polymer stress, we use the Oldroyd-B model, which is derived from treating polymer molecules as Hookean dumbbells. In this model, the elastic stress is described in terms of the conformation tensor $C_{ij} = \langle R_i R_j \rangle$, where R_i is the end-to-end vector of the elastic dumbbell representation of the polymer made nondimensional by the polymer's radius of gyration. The angle brackets represent the ensemble average. The nondimensional constitutive evolution equation is as follows:

$$\sigma_{ij}^{\text{poly}} = \frac{1-\beta}{\text{Wi}}(C_{ij} - \delta_{ij}), \tag{5}$$

$$\frac{\partial C_{ij}}{\partial t} + \text{Wi}(u_k \nabla_k C_{ij} - \nabla_k u_i C_{jk} - \nabla_k u_j C_{ik}) + C_{ij} = \delta_{ij}, \tag{6}$$

where time is nondimensionalized by the polymer relaxation time λ and the Weissenberg number $\text{Wi} \equiv \lambda/\tau_c$ is a measure of fluid elasticity.

B. Dilute suspension rheology

We consider the bulk stress in a dilute suspension of noncolloidal, freely suspended spheres in a viscoelastic fluid. To calculate the stress in this suspension, we in general require the ensemble average over many suspension configurations; however, in the dilute case and assuming the suspension is statistically homogenous, we can, equivalently, average over a sufficiently large volume [7,13], giving the following expression:

$$\langle \sigma_{ij}^{\text{total}} \rangle = \frac{1}{V}\int_V \sigma_{ij}^{\text{total}}\, dV, \tag{7}$$

$$= \frac{1}{V}\left(\int_{V_f} \sigma_{ij}^{\text{total},f}\, dV + \int_{V_p} \sigma_{ij}^{\text{total},p}\, dV\right), \tag{8}$$

where $\sigma_{ij}^{\text{total}}$ is the total or Cauchy stress in the suspension and varies with position; V_f, V_p are respectively the fluid and particle volumes both nondimensionalized by a^3; and $\sigma_{ij}^{\text{total},f}$, $\sigma_{ij}^{\text{total},p}$ are the total stress in the fluid and particle domains, respectively.

Following previous analyses [7], this bulk stress can be decomposed into separate components:

$$\langle \sigma_{ij}^{\text{total}} \rangle = \langle \sigma_{ij}^{\text{total},f0} \rangle + \phi(\Sigma_{ij} + S_{ij}), \tag{9}$$

$$\Sigma_{ij} = \frac{1}{V_p}\int_V \left(\sigma_{ij}^{\text{total},f} - \sigma_{ij}^{\text{total},f0}\right) dV, \tag{10}$$

$$S_{ij} = \frac{1}{V_p}\int_{A_p} x_j \sigma_{ik}^{\text{total},f} n_k\, dA = \frac{1}{V_p}\int_{A_p} x_j f_i\, dA, \tag{11}$$

where $\phi = V_p/V$ is the volume fraction of the particle in the suspension. The term $\sigma_{ij}^{\text{total},f0}$ in Eq. (9) is the stress of the suspending fluid subject to the same imposed "far-field" flow. For homogeneous shear or extensional flow in a single fluid phase, this stress is spatially invariant. The next two terms in Eq. (9) reflect separate contributions from the fluid and solid phases, respectively: Σ_{ij} PIFS and S_{ij} (the stresslet). Their definitions are as given in Eqs. (10) and (11); we have also assumed the

particles are force- and torque-free and have negligible inertial forces, allowing us to apply the divergence theorem and express the stresslet S_{ij} as an integral of moments of the traction over the particle surface.

The stresslet can further be decomposed into contributions arising from the three contributions to the fluid stress as shown in Eq. (3):

$$S_{ij} = \frac{1}{V_p}\left[\int_{A_p} -pn_i x_j \, dA + \int_{A_p} f_i^{\text{visc}} x_j \, dA + \int_{A_p} f_i^{\text{poly}} x_j \, dA\right], \tag{12}$$

$$= S_{ij}^{\text{pres}} + S_{ij}^{\text{visc}} + S_{ij}^{\text{poly}}, \tag{13}$$

$$f_i^{\text{visc}} = 2\beta E_{ik} n_k; \; f_i^{\text{poly}} = \frac{1-\beta}{\text{Wi}}(C_{ik} - \delta_{ik})n_k. \tag{14}$$

The effective per-particle viscosity η_{eff} indicates the additional stress created by the presence of a particle and, for shear and uniaxial extension, is defined as follows:

$$\eta_{\text{eff,shear}} = \frac{1}{\phi}\left(\frac{\langle\sigma_{12}\rangle}{\sigma_{12}^{f0}} - 1\right) = \Sigma_{12} + S_{12}, \tag{15}$$

$$\eta_{\text{eff,extension}} = \frac{1}{\phi}\left(\frac{\langle\sigma_{\text{ext}}\rangle}{\sigma_{\text{ext}}^{f0}} - 1\right) = \frac{\Sigma_{\text{ext}} + S_{\text{ext}}}{\sigma_{\text{ext}}^{f0}}, \tag{16}$$

$$(\cdot)_{\text{ext}} = (\cdot)_{11} - \frac{(\cdot)_{22} + (\cdot)_{33}}{2}, \tag{17}$$

where Eq. (17) applies to uniaxial extension with x_1 being the extensional axis. σ_{ext}^{f0} is the uniaxial extensional stress for an Oldroyd-B fluid, made dimensionless by the stress scale $\eta_0\dot{\epsilon}$, and is given as follows:

$$\sigma_{\text{ext}}^{f0} = 3\beta + \frac{1-\beta}{\text{Wi}}\left\{\frac{1 - 2\text{Wi}\exp\left[-(1-2\text{Wi})t\right]}{1-2\text{Wi}} - \frac{1 + \text{Wi}\exp\left[-(1+\text{Wi})t\right]}{1+\text{Wi}}\right\}. \tag{18}$$

The stresslet contribution to the effective viscosity has different forms for shear and extension, as follows:

$$\eta_{\text{stresslet,shear}} = S_{12} = S_{12}^{\text{pres}} + S_{12}^{\text{visc}} + S_{12}^{\text{poly}}, \tag{19}$$

$$\eta_{\text{stresslet,extension}} = \frac{S_{\text{ext}}}{\sigma_{\text{ext}}^{f0}} = \frac{S_{\text{ext}}^{\text{pres}} + S_{\text{ext}}^{\text{visc}} + S_{\text{ext}}^{\text{poly}}}{\sigma_{\text{ext}}^{f0}}. \tag{20}$$

For a Newtonian suspension, the total effective viscosity arises solely from the stresslet, as the PIFS is zero, and we recover the Einstein result for both shear and uniaxial extension:

$$\eta_{\text{eff,Newt}} = \eta_{\text{stresslet,Newt}} = 2.5. \tag{21}$$

C. The stresslet in the $\beta \to 1$ limit

In the limit of $\beta \to 1$, the suspending fluid approaches a Newtonian fluid. In the Stokes limit with $\text{Re} \to 0$, the pressure and velocity fields for a sphere in a general linear flow are known analytically [19]:

$$p = -\frac{5x_i E_{ij}^{\infty} x_j}{r^5}, \tag{22}$$

$$u_i = E_{ij}^{\infty} x_j\left(1 - \frac{1}{r^5}\right) + \Omega_{ij}^{\infty} x_j - x_i\left(x_j E_{jk}^{\infty} x_k\right)\left(\frac{5}{2r^5} - \frac{5}{2r^7}\right). \tag{23}$$

$$r = (x_k x_k)^{1/2}. \tag{24}$$

This allows us to calculate S_{ij}^{pres} and S_{ij}^{visc} directly, and detailed solutions are presented in Appendix A. To calculate S_{ij}^{poly}, an expression for $\sigma_{ij}^{\text{poly}}$, and hence C_{ij}, is required; detailed solutions are presented in Appendix B. In brief, the Oldroyd-B evolution equation is solved on the surface of the spherical particle, to derive equations for the components of C_{ij} that contribute to the surface tractions f_i^{poly}.

1. The stresslet in shear flow

The three components of the shear stresslet in Eq. (19) are required to get an expression for the effective per-particle viscosity in shear. We assume the pressure contribution S_{12}^{pres} as given by Eq. (A7) for a Newtonian suspending fluid remains constant with increasing Wi. S_{12}^{visc} was derived for a Newtonian fluid (i.e., $\beta = 1$) in Appendix A 1; since an Oldroyd-B fluid has dimensionless solvent viscosity $\beta < 1$, we scale Eq. (A4) by a factor of β. Finally, S_{12}^{poly} is given by Eq. (B32), as derived in Appendix B 1. Combining these results, the stresslet contribution to the effective per-particle viscosity for shear is given by

$$\eta_{\text{stresslet,shear}} = 1 + 1.5\beta + \frac{1.5(1-\beta)}{1+\text{Wi}^2}. \tag{25}$$

In Sec. III A, we compare these predicted scalings for the per-particle viscosity and constituents against results from simulations.

2. The stresslet in extensional flow

The three components of the extensional stresslet in Eq. (20) are required to get an expression for the effective per-particle viscosity in extension. $S_{\text{ext}}^{\text{visc}}$ was derived for a Newtonian fluid (i.e., $\beta = 1$) in Appendix A 2; since an Oldroyd-B fluid has dimensionless solvent viscosity $\beta < 1$, we scale Eq. (A10) by a factor of β. $S_{\text{ext}}^{\text{poly}}$ is given by Eq. (B41), as derived in Appendix B 2.

The pressure contribution $S_{\text{ext}}^{\text{pres}}$ is harder to quantify, as the pressure field evolves transiently everywhere in the fluid domain. Here we propose a scaling based on analysis of the fluid behavior on the sphere surface. The form of Eq. (B36) indicates the polymer locally experiences shear flow with a shear rate that depends on polar angle but is constant in time. Thus, the fluid on the surface of the sphere reacts like an initially quiescent Oldroyd-B fluid exposed to a step shear rate. From the transient shear stress growth of an Oldroyd-B fluid [20], the nondimensional transient shear viscosity is $\beta + (1-\beta)[1 - \exp(-t)]$. Assuming this increased viscosity on the particle surface dominates the evolution of the pressure contribution to the extensional stresslet, $S_{\text{ext}}^{\text{pres}}$ would evolve as follows:

$$S_{\text{ext}}^{\text{pres}} = 3[\beta + (1-\beta)(1-e^{-t})], \tag{26}$$

which corresponds to the Newtonian value [Eq. (A9)] scaled by a transiently thickening viscosity. Combining these results, the extensional stresslet (made nondimensional by the zero-shear viscosity) is given by:

$$S_{\text{ext}} = 7.5[\beta + (1-\beta)(1-e^{-t})], \tag{27}$$

and the stresslet contribution to the effective per-particle viscosity for uniaxial extension is thus:

$$\eta_{\text{stresslet,extension}} = \frac{7.5[\beta + (1-\beta)(1-e^{-t})]}{3\beta + \frac{1-\beta}{\text{Wi}}\left[\frac{1-2\text{Wi}\,e^{-(1-2\text{Wi})t}}{1-2\text{Wi}} - \frac{1+\text{Wi}\,e^{-(1+\text{Wi})t}}{1+\text{Wi}}\right]}. \tag{28}$$

In Sec. III B, we compare these predicted scalings for the per-particle viscosity and constituents against results from simulations.

D. The stresslet for $\beta < 1$: Direct numerical simulations

As the parameter β decreases, the polymer contribution to the stress in the fluid increases and the flow field increasingly deviates from the Newtonian results. The polymer conformation evolution Eq. (6) can no longer be evaluated exactly analytically in this regime. We turn to simulations to examine the stresslet for $\beta < 1$ in both shear and extension.

For simulations of shear flow, a neutrally buoyant sphere is placed at the center of a cubic computation domain of side length L in a macroscopic flow field $u_i = \dot{\gamma} x_2 \delta_{i1}$, where $\dot{\gamma}$ is the shear rate. Periodic conditions are imposed in the flow direction x_1 and the vorticity direction x_3. Shear flow is applied by imposing walls at $x_2 = \pm\frac{L}{2}$ moving at equal and opposite speeds $\pm U\delta_{i1}$. L is selected such that bulk shear flow is recovered far from the particles, and U is selected to achieve the desired shear rate $\dot{\gamma} = \frac{U}{L}$. The translational velocity of the sphere is zero by symmetry, and the rotational frequency is determined to maintain the torque-free condition.

For simulations of uniaxial extensional flow, a neutrally buoyant sphere is placed at the center of a cubic computation domain of side length L in a mean flow field $\langle u_i \rangle = \dot{\epsilon} \begin{pmatrix} x_1 \\ -x_2/2 \\ -x_3/2 \end{pmatrix}$, where $\dot{\epsilon}$ is the extension rate and x_1 is the extensional axis. Extensional flow is applied by imposing this velocity at the domain boundaries, based on the desired extension rate. L is selected such that bulk extensional flow is recovered far from the particles. The translational velocity and rotational frequency of the sphere are both zero by symmetry. We note that this approach only works for Wi < 0.5 for the Oldroyd-B fluid, such that the polymer stress at the domain boundaries corresponds to that of the homogenous bulk flow for a sufficiently large domain; for increased fluid elasticity, a different semianalytical approach can be employed [11] to accurately compute the polymer stress field.

The domain is discretized with a tetrahedral mesh that is finest on the surface of the sphere and coarsens with distance away from the sphere. The governing equations are solved using a massively parallel finite-volume flow solver developed at Stanford's Center for Turbulence Research [21]. Details of the solver and previous validation and convergence tests can be found in past publications [7,10,22]. From the simulations, we obtain the fluid velocity, pressure, and polymer stress everywhere in the computation domain. The stresslet is calculated from these quantities using Eq. (12).

III. RESULTS AND DISCUSSION

A. Shear flow

We carry out simulations with varying Wi at a fixed $\beta = 0.68$, to compare against previous results reported for a stresslet in a Giesekus fluid at the same value of β [7,14]. We decompose the stresslet into the pressure, viscous, and polymer contributions as described in Eq. (12). Figure 1 shows that as the elasticity of the suspending fluid increases, the stresslet decreases for an Oldroyd-B fluid, as it does for the Giesekus fluid reported previously [7,14]. The stresslet contributions further shows that the overall shear-thinning behavior is driven by a decrease in the polymer contribution to the stresslet. In the same plot, we compare the simulation results to theoretical scaling predictions as detailed in Sec. II C 1, Eq. (25). We see good agreement between simulation and theory results up to Wi <1. As Wi increases, the total shear stresslet increasingly deviates from the predicted scaling. This is expected as the scaling was derived for the Newtonian flow field [Eq. (23)]; as Wi increases, the velocity and pressure increasingly deviate from the Newtonian results, which can lead to the deviation observed at higher Wi.

We provide a physical explanation for the decreasing polymer stresslet by considering a packet of fluid on the surface of the sphere in a Lagrangian reference frame. As the freely suspended sphere rotates in shear, a packet of fluid on the surface travels in the azimuthal direction on a trajectory of constant θ, and reacts to the velocity gradients it samples along that trajectory. Equation (B22) corresponds to the same governing equations as an Oldroyd-B fluid exposed to oscillating shear flow between parallel plates; converting to the Lagrangian view, as the packet of fluid goes from

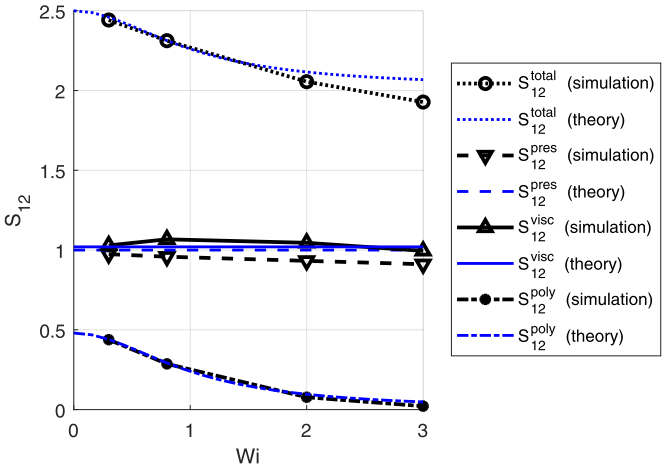

FIG. 1. Comparison of results from theory [Eq. (25)] and simulations for the stresslet and component contributions to the effective shear viscosity with changing Wi, $\beta = 0.68$.

$\phi = 0$ to $\phi = \pi$, it experiences and reacts to a shear rate in the azimuthal direction which oscillates one full cycle with magnitude $\frac{5}{2}\sin\theta$. The azimuthal polymer traction, obtained by projecting the polymer traction [Eq. (B7)] along the azimuthal direction, hence corresponds to the shear tractions exerted in the case of oscillating parallel plates:

$$\hat{\phi}_i = \begin{pmatrix} -\sin\phi \\ \cos\phi \\ 0 \end{pmatrix}, \tag{29}$$

$$f_\phi^{\text{poly}} = \hat{\phi}_i f_i^{\text{poly}} = \frac{5\sin\theta}{2}\frac{(1-\beta)}{1+\text{Wi}^2}(\cos 2\phi - \text{Wi}\sin 2\phi), \tag{30}$$

$$= \frac{5\sin\theta(1-\beta)}{2}\frac{1}{\sqrt{1+\text{Wi}^2}}\cos(2\phi + \Delta\phi);\ \Delta\phi = \arctan(-\text{Wi}). \tag{31}$$

Similarly, Eq. (B21) also corresponds to the same governing equations as an Oldroyd-B fluid exposed to oscillating shear flow between parallel plates; however, the shear rate is now in the *polar* direction and has magnitude $\frac{5}{4}\sin 2\theta$. The *polar* polymer traction hence also corresponds to the shear tractions exerted in the case of oscillating parallel plates:

$$\hat{\theta}_i = \begin{pmatrix} \cos\theta\cos\phi \\ \cos\theta\sin\phi \\ \cos\theta \end{pmatrix}, \tag{32}$$

$$f_\theta^{\text{poly}} = \hat{\theta}_i f_i^{\text{poly}} = \frac{5\sin 2\theta}{4}\frac{(1-\beta)}{1+\text{Wi}^2}(\cos 2\phi - \text{Wi}\sin 2\phi), \tag{33}$$

$$= \frac{5\sin 2\theta(1-\beta)}{4}\frac{1}{\sqrt{1+\text{Wi}^2}}\cos(2\phi + \Delta\phi);\ \Delta\phi = \arctan(-\text{Wi}). \tag{34}$$

Equations (31) and (34) show the azimuthal and polar polymer tractions are sinusoidal, with a phase shift that increases as Wi increases. The amplitude of these tractions scale as $\frac{1}{\sqrt{1+\text{Wi}^2}}$; i.e., the maximum and minimum polymer tractions on the surface of the particle scales as $\mathcal{O}(\text{Wi}^{-1})$ and decrease as Wi increases. However, Eq. (B32) shows that the stresslet scales as $\mathcal{O}(\text{Wi}^{-2})$—this arises as the stresslet is the integral of the moment of the traction on the surface of the sphere.

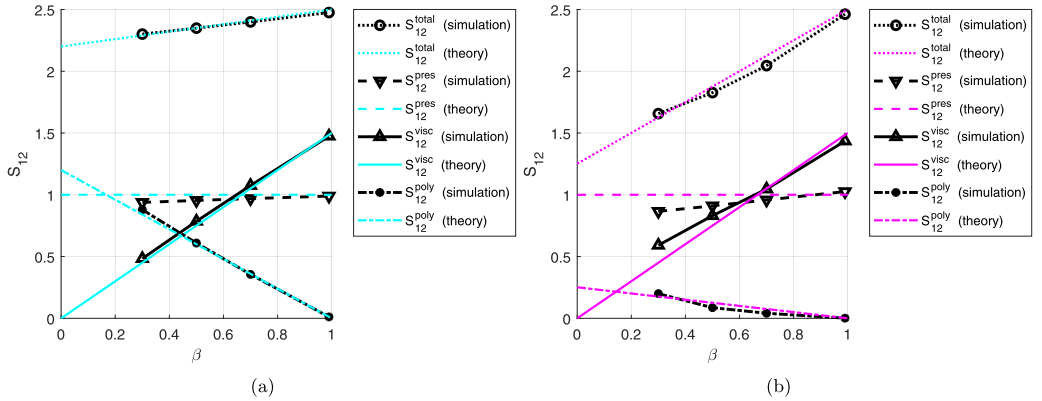

FIG. 2. Comparison of results from theory [Eq. (25)] and simulations for the stresslet and component contribution to the effective shear viscosity, as a function of β. (a) Wi $= 0.5$; (b) Wi $= 2.2297$.

Physically, the finite relaxation time of the polymer causes a packet of fluid on the surface of the sphere to have a delay in reacting to the shear rate it experiences; the packet of fluid reacts to a temporally averaged shear rate over a time period proportional to the polymer reaction time. This temporally averaged shear rate is of smaller magnitudes than the instantaneous oscillating shear rate, hence leading to the decreased surface tractions observed.

To investigate the range of β for which the scaling derived in Eq. (25) is valid, simulations were performed at two fixed Wi for a range of β values, and the resultant stresslet and component contributions plotted against β (Fig. 2). It can be seen that as β decreases, the scaling of the polymer contribution retains good agreement with Eq. (25). At the higher value of Wi [Fig. 2(b)], deviations in the polymer and viscous contributions to the stresslet become more significant, which is again attributed to stronger deviations in the velocity and pressure fields from the Newtonian result as β decreases.

B. Extensional flow

Extensional simulations were carried out with an Oldroyd-B fluid for Wi $= 0.2$ and 0.4 at a fixed $\beta = 0.68$ as studied previously [10]. Figure 3 shows simulation results for the extensional

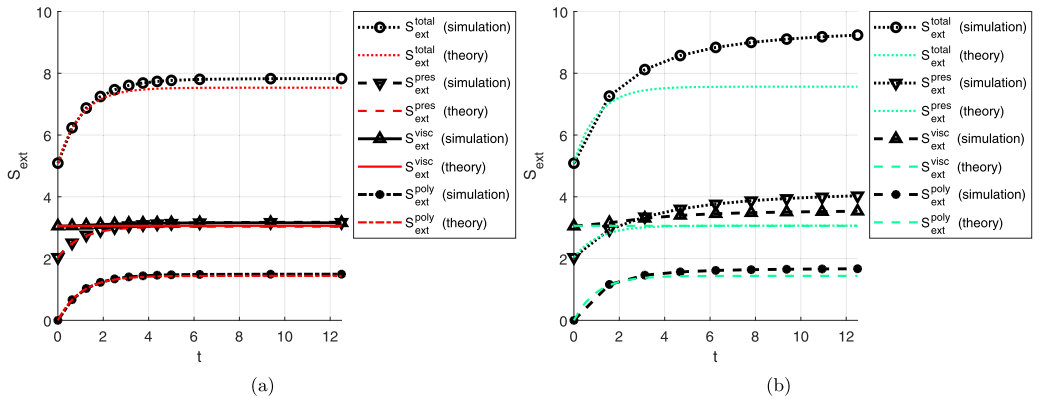

FIG. 3. Comparison of results from theory [Eq. (27)] and simulations for extensional stresslet and components at $\beta = 0.68$, with time nondimensionalized by the polymer relaxation time λ. (a) Wi $= 0.2$; (b) Wi $= 0.4$.

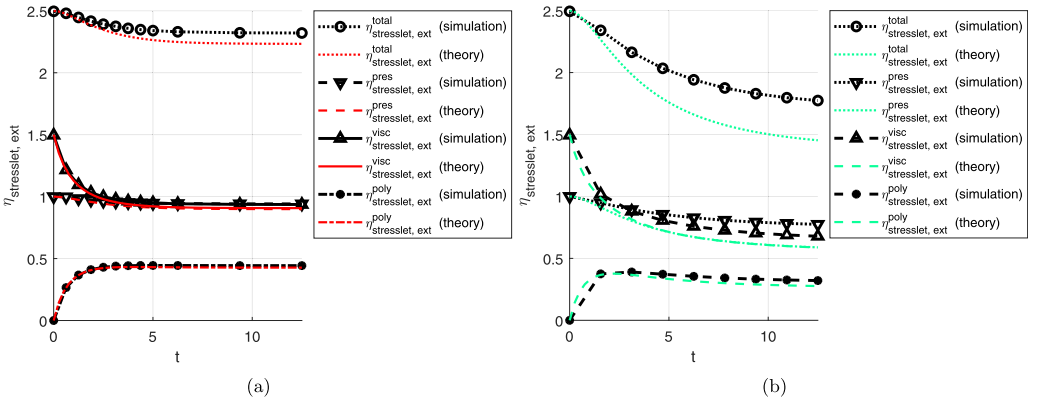

FIG. 4. Comparison of results from theory [Eq. (28)] and simulation for extensional stresslet contributions to the effective viscosity at $\beta = 0.68$, with time nondimensionalized by the polymer relaxation time λ. (a) Wi $= 0.2$; (b) Wi $= 0.4$.

stresslet and its components, compared to the theoretical scalings derived in Sec. II C 2. The transient evolution of the stresslet components shows good agreement at lower Wi [Fig. 3(a)]; the simulation results show a larger extensional stresslet than predicted by theory, driven by higher pressure and viscous contributions. These deviations increase in magnitude at the higher Wi of 0.4 [Fig. 3(b)]. The deviation in the pressure contribution, in particular, is likely due to changes in the fluid stress away from the particle surface, which are not captured by our scaling argument for the viscosity at the particle surface. Previous studies [10,11] analyzed velocity gradients in the region of the fluid near the particle and found regions of strong extensional flow, which create larger gradients in the polymer stress. These can then contribute to stronger deviations in the pressure and velocity fields as compared to the Newtonian result.

Figure 4 shows the stresslet contribution to the effective extensional viscosity, which is the extensional stresslet scaled by the (transient) extensional stress of the suspending fluid alone. The initial value of 2.5 at $t = 0$ arises as the Newtonian component of the suspending fluid reacts instantaneously in the Stokes limit, for both the suspension and the suspending fluid, and so the pressure and viscous components adopt their Newtonian values at $t = 0$. However, the polymer component has a finite relaxation time and so evolves for $t > 0$. We note that even though $\eta^{total}_{stresslet,\,ext}$

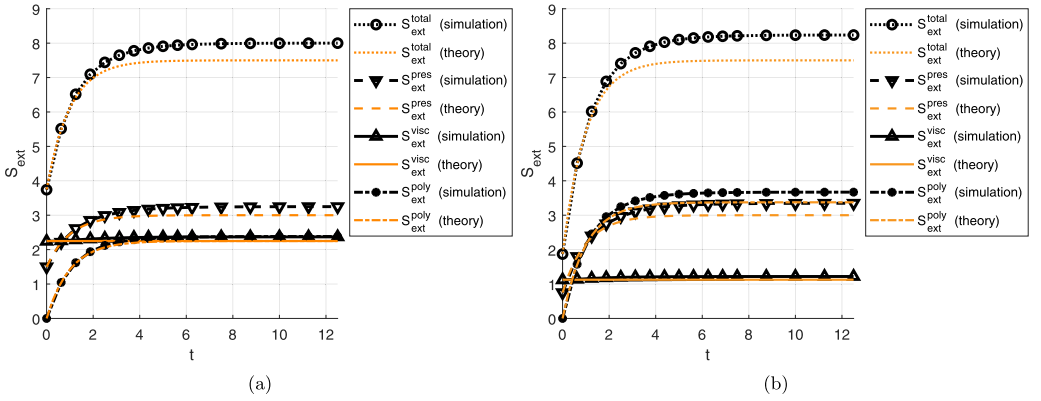

FIG. 5. Comparison of results from theory [Eq. (27)] and simulations for extensional stresslet and components at Wi $= 0.2$, with time nondimensionalized by the polymer relaxation time λ. (a) $\beta = 0.50$; (b) $\beta = 0.25$.

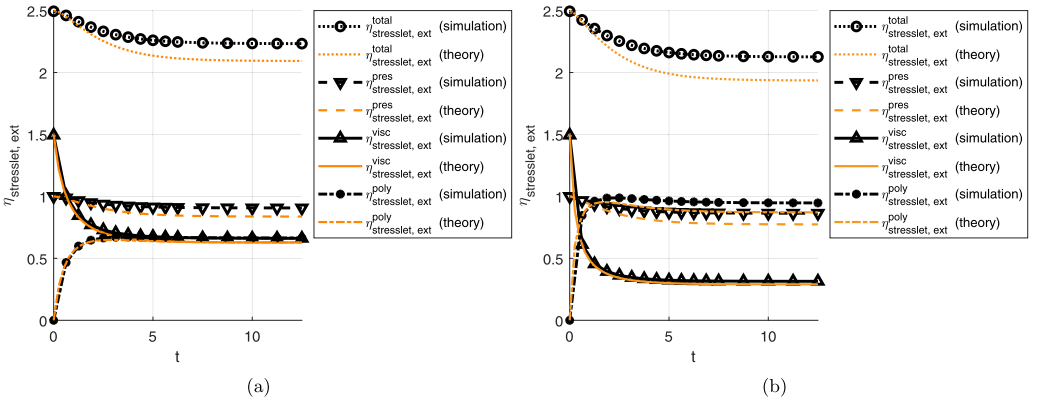

FIG. 6. Comparison of results from theory [Eq. (28)] and simulation for extensional stresslet contributions to the effective viscosity at Wi $= 0.2$, with time nondimensionalized by the polymer relaxation time λ. (a) $\beta = 0.50$; (b) $\beta = 0.25$.

decreases over time, the actual extensional stresslet $S^{\text{total}}_{\text{ext}}$ increases, indicating the surface tractions increase with time. This is in contrast to the case of shear (Sec. III A), where the decreasing effective viscosity indicates a decrease in surface tractions. The decreasing trend in $\eta^{\text{total}}_{\text{stresslet, ext}}$ should rather be interpreted as the particle creating regions of shear flow on its surface, causing the evolution of the stress in the particle domain to be decreased relative to regions of extensional flow outside.

To investigate the range of β for which these scalings are valid in extensional flow, simulations were performed at Wi $= 0.2$ for two β values. Figure 5 shows the effect of decreasing β on the extensional stresslet. Comparing Figs. 3(a), 5(a), and 5(b), we see that decreasing β causes the deviations at long elastic times to increase, driven mostly by deviations in the pressure contribution. Again, we attribute these to increasing changes in the pressure and velocity fields external to the particle as β decreases. Finally, Fig. 6 shows the effect of decreasing β on the stresslet contribution to the extensional per-particle viscosity, with the same trends as the extensional stresslet when comparing the simulation results to the theoretical scaling.

IV. CONCLUSIONS

The stresslet contribution to the effective shear and extensional viscosities of a dilute suspension of spheres in an Oldroyd-B fluid was considered both analytically and through direct numerical simulations. The analytical expressions were derived in the limit of a Newtonian flow field, valid when $\beta = 1$, and only accounts for stress contributions on the particle surface. Hence the equations presented here are not rigorously asymptotic in the limit $1 - \beta \to 0$; the reader is directed to references in the following subsections for more complete investigations in that limit for shear and extensional flow, respectively. The trends in these contributions, as well as the origin for these observed trends, were found to be different in each type of flow.

A. Shear flow

For dilute suspensions of rigid spheres under imposed shear in an Oldroyd-B fluid, simulations at finite β showed that the tractions exerted by the polymer component on the surface of the sphere decreased with increasing fluid elasticity, and this effect dominated the overall shear-thinning behavior of the stresslet. Polymer tractions in the limit of the Newtonian flow field were analyzed along fluid streamlines on the surface of the sphere—these correspond to trajectories of constant radius and polar angle in spherical coordinates. It was found that along these streamlines, the polymer traction is driven by oscillations of the shear rate along the azimuthal and polar directions. The resultant polymer tractions are phase shifted by an amount proportional to the elasticity (relaxation time)

of the polymer. The exact form of these tractions is given by the linear viscoelastic response to oscillatory shear.

A scaling for the stresslet contribution to the effective shear viscosity is found for the Newtonian flow field limit, and simulations at decreasing β showed that the polymer component of the stresslet is well described by this scaling. The pressure and viscous contributions to the stresslet exhibit deviations from the scaling given by Eqs. (A7) and (A4) respectively, and these deviations increase with increasing Wi. The scaling with Wi [Eq. (25)] can be compared with earlier perturbation analysis of the effective viscosity of a dilute suspension of rigid spheres in a second-order fluid, with Wi as the small parameter [23]. It was reported that the leading order effect on the effective viscosity is $\mathcal{O}(\mathrm{Wi}^2)$, which agrees with an expansion of Eq. (25) for low Wi. A possible cause for these deviations is that the velocity and pressure fields undergo stronger deviations from the Newtonian fields; lowering β and increasing Wi both lead to larger deviations in these fields, which in turn could lead to changes in the surface tractions and hence the stresslet contributions. The effects of such deviations in the velocity and pressure fields on the effective viscosity are considered in greater detail in previous work [5]: This contribution is seen to remain roughly constant up to Wi $= 1$ in the limit of low polymer concentration.

We can use these results to predict the stress experienced by dilute spherical particles in a macroscopic shear flow, with a Newtonian suspending fluid versus a Boger fluid—an experimental fluid with shear behavior well described by the Oldroyd-B—of the same zero-shear viscosity. Due to the mechanism proposed above for the polymer tractions on the particle surface, the particles suspended in the Boger fluid are expected to experience lower shear stresses than those suspended in the Newtonian fluid. Alternatively, this mechanism can be interpreted by considering the Lagrangian history of the shear rate experienced by a packet of fluid on the particle surface: Such a packet of fluid reacts to a temporally averaged shear rate over a time period proportional to the polymer reaction time. The oscillating instantaneous shear rate leads to a temporally averaged shear which also oscillates, but has a smaller amplitude, hence leading to the decreased surface tractions observed. This reduction in shear stress can be the mechanism that causes soft particles to deform less when sheared under the same shear rate in a Boger fluid than in a Newtonian fluid, when both fluids have the same zero-shear viscosity [24].

B. Extensional flow

For dilute suspensions of rigid spheres under imposed uniaxial extension in an Oldroyd-B fluid where Wi <0.5, simulations at finite β showed that the contributions of pressure and polymer tractions to the extensional viscosity both increased with the startup of strain, while the contribution of viscous tractions remains mostly constant. Polymer tractions in the limit of the Newtonian flow field limit were analyzed on the stationary surface of the sphere. It was found that the Oldroyd-B fluid on the surface of the sphere experiences constant shear in the polar direction, with magnitude dependent on the polar angle. The transient response of the surface polymer tractions thus corresponds to the transient (start-up) shear response of an Oldroyd-B fluid, and the polymer contribution to the stresslet can evaluated accordingly.

The pressure contribution to the stresslet can only be evaluated completely with knowledge of the polymer behavior in the whole fluid domain. However, as a first approximation, the pressure contribution can be assumed to be dominated by the increase in viscosity of the fluid on the sphere surface.

A scaling for the stresslet effective extensional viscosity was found for the Newtonian flow field limit. Simulations at decreasing β showed that the proposed scaling underpredicts results from simulations, with the largest deviation arising from the pressure contribution. The simulation results deviate more strongly with increasing Wi and decreasing β, i.e., as the fluid becomes increasingly non-Newtonian, larger deviations in the pressure and velocity fields from the Newtonian result are expected. In particular, particles in a macroscopic extensional flow generate regions of strong extension around it, leading to larger gradients in the polymer stress that can exacerbate deviations

in the pressure and velocity fields. A thorough investigation of how suspending fluid viscoelasticity affects the stresslet in steady extensional flow, taking these deviations into account, can be found in previous work [11]. Perturbation analyses of the steady effective extensional viscosity of a dilute suspension of rigid spheres in a second-order fluid, with Wi as the small parameter, have also been reported in the literature [23,25,26].

While the effective stresslet extensional viscosity is reported to decrease with increasing Wi at the same strain, it should be noted that the tractions on the surface of the particle increase transiently with elastic time (e.g., as shown in Fig. 3). As in Sec. IV A, we compare suspensions of dilute spherical particles with a Newtonian suspending fluid versus a Boger fluid of the same zero-shear viscosity, now in a macroscopic uniaxial extensional flow. The tractions at $t = 0$ are lower at $t = 0$ with the Boger suspending fluid than the Newtonian, and these tractions increase on the timescale of the polymer relaxation time. With a Newtonian flow field, the surface shear tractions in the Boger fluid case increase up to a steady value that equals those from the Newtonian suspending fluid. The particle then experiences lower shear tractions for some time in the Oldroyd-B fluid compared to the Newtonian fluid, which might be relevant in applications, depending on the duration of applied extension. However, the pressure tractions from simulation are higher than predicted from theory, indicating increased normal tractions on the particle surface in the Boger fluid as compared to the Newtonian fluid.

ACKNOWLEDGMENTS

This work was supported by the National Science Foundation Grant No. CBET 1803765. N.B.S. is supported by the Agency of Science Technology and Research, Singapore (A*STAR) NSS-PhD award. The computations in this paper were performed on the Yellowstone cluster at the Stanford HPC Center, supported through awards from Intel, National Science Foundation, DOD HPCMP, and Office of Naval Research.

APPENDIX A: PRESSURE AND VISCOUS CONTRIBUTIONS TO THE EFFECTIVE VISCOSITY

Equation (12) can be used to calculate the pressure and viscous stresslet contributions, S_{ij}^{pres} and S_{ij}^{visc}, respectively, in shear and extension. We evaluate these for a Newtonian fluid, i.e., for $\beta = 1$.

1. Pressure and viscous stresslet in shear

To evaluate Eq. (12) directly, we adopt a spherical coordinate system with the polar axis aligned to the vorticity axis and the azimuthal axis aligned to the flow direction. Equations (22) and (23) give the pressure and velocity fields respectively in this $\beta = 1$ limit, with $E_{ij}^{\infty} = \frac{1}{2}(\delta_{i1}\delta_{j2} + \delta_{j1}\delta_{i2})$ and $\Omega_{ij}^{\infty} = \frac{1}{2}(\delta_{i1}\delta_{j2} - \delta_{j1}\delta_{i2})$. However, since only the macroscopic rate-of-strain leads to a stresslet, we set $\Omega_{ij}^{\infty} = 0$ in Eq. (23), then evaluate E_{ij} on the sphere surface and subsequently S_{ij}^{visc}:

$$f_i^{\text{visc}} = 2E_{ij}n_j\Big|_{\text{surface}} \tag{A1}$$

$$= \begin{bmatrix} \frac{5}{2}\sin\phi\sin\theta(2\sin\phi\sin^2\theta - 2\sin^2\theta + 1) \\ \frac{1}{16}(25\cos\phi\sin\theta + 15\cos 3\phi\sin\theta + 5\sin 3\theta\cos\phi - 5\cos 3\phi\sin 3\theta) \\ \frac{5}{2}\sin 2\phi\cos\theta(\cos^2\theta - 1) \end{bmatrix}, \tag{A2}$$

$$n_i = x_i\Big|_{\text{surface}} = \begin{bmatrix} \cos\phi\sin\theta \\ \sin\phi\sin\theta \\ \cos\theta \end{bmatrix}, \tag{A3}$$

$$S_{12}^{\text{visc}} = \frac{3}{4\pi}\int_0^{\pi}\int_0^{2\pi} f_1^{\text{visc}}x_2\,\sin\theta d\phi d\theta = 1.5. \tag{A4}$$

The pressure tractions can similarly be evaluated:

$$p = \frac{5}{4}\sin 2\phi(\cos 2\theta - 1), \tag{A5}$$

$$n_i = x_i\Big|_{\text{surface}} = \begin{pmatrix}\cos\phi\sin\theta\\ \sin\phi\sin\theta\\ \cos\theta\end{pmatrix}, \tag{A6}$$

$$S_{12}^{\text{pres}} = \frac{3}{4\pi}\int_0^{\pi}\int_0^{2\pi} -pn_1x_2\,\sin\theta d\phi d\theta = 1. \tag{A7}$$

The effective per-particle viscosity $\eta_{\text{effective, Newt}} = S_{12}^{\text{pres}} + S_{12}^{\text{visc}} = 2.5$, recovering the Einstein viscosity. These results agree with those obtained by Koch *et al.* [5] in the limit of $\text{De} = 0$ in their text, obtained by a different analysis using a perturbation expansion.

2. Pressure and viscous stresslet in uniaxial extension

To evaluate surface tractions, We apply the same procedure as the preceding Sec. (A 1), but adopting a spherical coordinate system with the polar axis aligned to the extensional axis instead, and setting $E_{ij}^{\infty} = \delta_{i1}\delta_{j1} - 0.5\delta_{i2}\delta_{j2} - 0.5\delta_{i3}\delta_{j3}$ and $\Omega_{ij}^{\infty} = 0$ in Eqs. (22) and (23). This leads to the following tensors for the two stresslet contributions:

$$S_{ij}^{\text{pres}} = \begin{pmatrix}2 & 0 & 0\\ 0 & -1 & 0\\ 0 & 0 & -1\end{pmatrix}; \quad S_{ij}^{\text{visc}} = \begin{pmatrix}3 & 0 & 0\\ 0 & -1.5 & 0\\ 0 & 0 & -1.5\end{pmatrix}. \tag{A8}$$

Evaluating Eq. (20) for the pressure and viscous contributions, noting that $\sigma_{\text{ext}}^{f0} = 3$ (a.k.a. the Trouton ratio) for Newtonian uniaxial extension:

$$S_{\text{ext}}^{\text{pres}} = 3; \eta_{\text{pres, Newt}} = 1, \tag{A9}$$

$$S_{\text{ext}}^{\text{visc}} = 4.5; \eta_{\text{visc, Newt}} = 1.5. \tag{A10}$$

As in Sec. A 1, the pressure contributes a value of 1 and the viscous tractions contribute a value of 1.5 to the effective per-particle viscosity, and the total value of 2.5 is the Einstein viscosity result.

APPENDIX B: ANALYTICAL SOLUTIONS TO OLDROYD-B EVOLUTION EQUATIONS ON THE SURFACE OF THE SPHERE

We use the hyperbolic nature of the Oldroyd-B equation to evaluate the polymer stress on the surface of the sphere in either shear or uniaxial extension. Due to the geometry of the problem, we evaluate the Oldroyd-B equation in spherical coordinates in both cases. In general, this is given by the following form:

$$\frac{\partial \underline{\underline{C}}^{\text{sph}}}{\partial t} + \text{Wi}\left\{\vec{u}^{\text{sph}}\cdot(\vec{\nabla}\underline{\underline{C}})^{\text{sph}} + (\vec{\nabla}\vec{u})^{\text{sph}}\cdot\underline{\underline{C}}^{\text{sph}} + \left[(\vec{\nabla}\vec{u})^{\text{sph}}\cdot\underline{\underline{C}}^{\text{sph}}\right]^T\right\} + \underline{\underline{C}}^{\text{sph}} = \underline{\underline{I}}, \tag{B1}$$

$$\underline{\underline{C}}^{\text{sph}} = \begin{pmatrix}C_{rr} & C_{r\theta} & C_{r\phi}\\ C_{r\theta} & C_{\theta\theta} & C_{\theta\phi}\\ C_{r\phi} & C_{\theta\phi} & C_{\phi\phi}\end{pmatrix}. \tag{B2}$$

1. Polymer stresslet in shear

We consider a freely suspended particle in a macroscopic steady shear flow, given in nondimensional terms as:

$$u_i^{\infty} = \delta_{i1}x_2. \tag{B3}$$

Equation (23) gives the velocity field in this $\beta = 1$ limit, with $E_{ij}^{\infty} = \frac{1}{2}(\delta_{i1}\delta_{j2} + \delta_{j1}\delta_{i2})$ and $\Omega_{ij}^{\infty} = \frac{1}{2}(\delta_{i1}\delta_{j2} - \delta_{j1}\delta_{i2})$.

The polymer surface traction in Cartesian coordinates is required to evaluate the polymer stresslet [Eq. (12)]. It can be expressed in terms of $\underline{\underline{C}}^{\text{sph}}$ as follows:

$$R_{ij} = \begin{pmatrix} \sin\theta\cos\phi & \sin\theta\sin\phi & \cos\theta \\ \cos\theta\cos\phi & \cos\theta\sin\phi & -\sin\theta \\ -\sin\phi & \cos\phi & 0 \end{pmatrix}, \tag{B4}$$

$$f_i^{\text{poly}} = \frac{1-\beta}{\text{Wi}}(C_{ij} - \delta_{ij})n_j, \tag{B5}$$

$$= \frac{1-\beta}{\text{Wi}}\left[\underline{\underline{R}}^T \cdot \left(\underline{\underline{C}}^{\text{sph}} - \underline{\underline{I}}\right) \cdot \underline{\underline{C}}\right] \cdot \vec{n}, \tag{B6}$$

$$= \frac{1-\beta}{\text{Wi}}\begin{bmatrix} C_{r\theta}\cos\phi\cos\theta - C_{r\phi}\sin\phi + (C_{rr}-1)\cos\phi\sin\theta \\ C_{r\phi}\cos\phi + C_{r\theta}\cos\theta\sin\phi + (C_{rr}-1)\sin\phi\sin\theta \\ -C_{r\theta}\sin\theta + (C_{rr}-1)\cos\theta \end{bmatrix}. \tag{B7}$$

We observe that only the $C_{rr}, C_{r\theta}, C_{r\phi}$ components contribute to the traction exerted by the polymer on the surface of the sphere. To get expressions for these components, we evaluate Eq. (B1) in spherical coordinates with the polar axis aligned to the vorticity axis and the azimuthal axis aligned to the flow direction. The partial time derivative is zero in the Eulerian steady case. The velocity gradient tensor $(\vec{\nabla}\vec{u})^{\text{sph}}$ can be evaluated via rotating the Cartesian velocity gradient tensor $\vec{\nabla}\vec{u}$:

$$(\vec{\nabla}\vec{u})^{\text{sph}} = \underline{\underline{R}}^T \cdot (\vec{\nabla}\vec{u}) \cdot \underline{\underline{R}}. \tag{B8}$$

The gradient of $\underline{\underline{C}}^{\text{sph}}$ also has to be evaluated. However, this can be simplified as we only evaluate Eq. (B1) on the surface of the sphere. In the Stokes limit, the sphere has dimensionless rotation rate $1/2$ along the vorticity axis; the velocity on the sphere surface is then:

$$\vec{u}^{\text{sph}} = \begin{pmatrix} u_r \\ u_\theta \\ u_\phi \end{pmatrix} = \begin{pmatrix} 0 \\ 0 \\ -1/2 \end{pmatrix}. \tag{B9}$$

Therefore, only the azimuthal gradient of $\underline{\underline{C}}^{\text{sph}}$ has to be evaluated. To do so, we express $\underline{\underline{C}}^{\text{sph}}$ as the sum of outer products of spherical basis vectors, and take azimuthal derivatives, using the notation $\partial_\phi(\cdot) \equiv \frac{\partial(\cdot)}{\partial\phi}$:

$$\underline{\underline{C}}^{\text{sph}} = C_{rr}\hat{r}\hat{r} + C_{r\theta}(\hat{r}\hat{\theta}_j + \hat{\theta}\hat{r}) + C_{r\phi}(\hat{r}\hat{\phi} + \hat{\phi}\hat{r}) + C_{\theta\theta}\hat{\theta}\hat{\theta} + C_{\theta\phi}(\hat{\theta}\hat{\phi} + \hat{\phi}\hat{\theta}) + C_{\phi\phi}\hat{\phi}\hat{\phi}, \tag{B10}$$

$$\partial_\phi\hat{r} = \sin\theta\hat{\phi};\ \partial_\phi\hat{\theta} = \cos\theta\hat{\phi};\ \partial_\phi\hat{\phi} = -\sin\theta\hat{r} - \cos\theta\hat{\theta}, \tag{B11}$$

$$\partial_\phi(\hat{r}\hat{r}) = \sin\theta\hat{\phi}\hat{r} + \sin\theta\hat{r}\hat{\phi}, \tag{B12}$$

$$\partial_\phi(\hat{r}\hat{\theta}) = \sin\theta\hat{\phi}\hat{\theta} + \cos\theta\hat{r}\hat{\phi}, \tag{B13}$$

$$\partial_\phi(\hat{\theta}\hat{r}) = \sin\theta\hat{\theta}\hat{\phi} + \cos\theta\hat{\phi}\hat{r}, \tag{B14}$$

$$\partial_\phi(\hat{r}\hat{\phi}) = \sin\theta\hat{\phi}\hat{\phi} - \sin\theta\hat{r}\hat{r} - \cos\theta\hat{r}\hat{\theta}, \tag{B15}$$

$$\partial_\phi(\hat{r}\hat{\phi}) = \sin\theta\hat{\phi}\hat{\theta} - \sin\theta\hat{r}\hat{r} - \cos\theta\hat{r}\hat{\theta}, \tag{B16}$$

$$\partial_\phi(\hat{\theta}\hat{\theta}) = \cos\theta\hat{\phi}\hat{\theta} + \cos\theta\hat{\theta}\hat{\phi}, \tag{B17}$$

$$\partial_\phi(\hat{\theta}\hat{\phi}) = \cos\theta\hat{\phi}\hat{\phi} - \sin\theta\hat{\theta}\hat{r} - \cos\theta\hat{\theta}\hat{\theta}, \tag{B18}$$

$$\partial_\phi(\hat{\phi}\hat{\phi}) = -\sin\theta\hat{r}\hat{\phi} - \cos\theta\hat{\theta}\hat{\phi} - \sin\theta\hat{\phi}\hat{r} - \cos\theta\hat{\phi}\hat{\theta}. \tag{B19}$$

Combining the above simplifications, we get the following system of six equations:

$$-\frac{\mathrm{Wi}}{2}\partial_\phi C_{rr} + C_{rr} = 1, \tag{B20}$$

$$-\frac{\mathrm{Wi}}{2}\partial_\phi C_{r\theta} + C_{r\theta} = \frac{5\mathrm{Wi}}{4}\sin 2\theta \sin 2\phi C_{rr}, \tag{B21}$$

$$-\frac{\mathrm{Wi}}{2}\partial_\phi C_{r\phi} + C_{r\phi} = \frac{5\mathrm{Wi}}{2}\sin\theta \cos 2\phi C_{rr}, \tag{B22}$$

$$-\frac{\mathrm{Wi}}{2}\partial_\phi C_{\theta\theta} + C_{\theta\theta} = 1 + \frac{5\mathrm{Wi}}{2}\sin 2\theta \sin 2\phi C_{r\theta}, \tag{B23}$$

$$-\frac{\mathrm{Wi}}{2}\partial_\phi C_{\theta\phi} + C_{\theta\phi} = \frac{5\mathrm{Wi}}{4}\sin 2\theta \sin 2\phi C_{r\phi} + \frac{5\mathrm{Wi}}{2}\sin\theta \cos 2\phi C_{r\theta}, \tag{B24}$$

$$-\frac{\mathrm{Wi}}{2}\partial_\phi C_{\phi\phi} + C_{\phi\phi} = 1 + 5\mathrm{Wi}\sin\theta \cos 2\phi. \tag{B25}$$

To solve for the three components of $\underline{\underline{C}}^{\mathrm{sph}}$ required to evaluate Eq. (B7), we solve Eqs. (B20), (B21), and (B22):

$$C_{rr} = 1, \tag{B26}$$

$$C_{r\phi} = \frac{5\mathrm{Wi}\sin\theta}{2}\left[\frac{1}{1+\mathrm{Wi}^2}\cos 2\phi - \frac{\mathrm{Wi}}{1+\mathrm{Wi}^2}\sin 2\phi\right], \tag{B27}$$

$$C_{r\theta} = \frac{5\mathrm{Wi}\sin 2\theta}{4}\left[\frac{1}{1+\mathrm{Wi}^2}\sin 2\phi + \frac{\mathrm{Wi}}{1+\mathrm{Wi}^2}\cos 2\phi\right]. \tag{B28}$$

The stresslet can now be calculated via Eq. (12); examining the shear (12) component of the stresslet:

$$S_{ij}^{\mathrm{poly}} = \frac{3}{4\pi}\int_{A_p} f_i^{\mathrm{poly}} x_j \, dA, \tag{B29}$$

$$x_i = \begin{pmatrix} \cos\phi \sin\theta \\ \sin\phi \sin\theta \\ \cos\theta \end{pmatrix}, \tag{B30}$$

$$S_{12}^{\mathrm{poly}} = \frac{3(1-\beta)}{4\pi\,\mathrm{Wi}}\int_0^{\pi}\int_0^{2\pi} (C_{r\theta}\cos\phi\cos\theta - C_{r\phi}\sin\phi)(\sin\theta\sin\phi)\,\sin\theta\, d\phi d\theta, \tag{B31}$$

$$= \frac{1.5(1-\beta)}{1+\mathrm{Wi}^2}. \tag{B32}$$

2. Polymer stresslet in uniaxial extension

We consider a freely suspended particle in a macroscopic uniaxial extensional flow, given in nondimensional terms as:

$$u_i^{\infty} = E_{ij}^{\infty} x_j, \tag{B33}$$

$$E_{ij}^{\infty} = \begin{pmatrix} 1 & 0 & 0 \\ 0 & -0.5 & 0 \\ 0 & 0 & -0.5 \end{pmatrix}. \tag{B34}$$

Equation (23) gives the velocity field in this $\beta = 1$ limit, with E_{ij}^{∞} as above and $\Omega_{ij}^{\infty} = 0$

As with Sec. B 1, the polymer surface tractions [Eq. (B7)] are required to evaluate S_{ij}. We again evaluate Eq. (B1) in spherical coordinates; this time, the polar axis is aligned to the extension axis x_1 with the specified form of E_{ij}^{∞}. The velocity gradient tensor $(\vec{\nabla}\vec{u})^{\text{sph}}$ is again evaluated via rotating the Cartesian velocity gradient tensor $\nabla_j u_i$. The particle is stationary and so the convective term is zero. In the $\beta = 1$ limit, the velocity field is steady; however, the polymer stress field can be transient, so the time-dependent term remains. For this flow field, the governing equations for the three C_{ij} components in Eq. (B7) are as follows:

$$\frac{\partial C_{rr}}{\partial t} + C_{rr} = 1, \tag{B35}$$

$$\frac{\partial C_{r\theta}}{\partial t} + C_{r\theta} = -\frac{15\text{Wi}}{4} \sin 2\theta C_{rr}, \tag{B36}$$

$$\frac{\partial C_{r\phi}}{\partial t} + C_{r\phi} = 0. \tag{B37}$$

Solving for these components:

$$C_{rr} = 1, \tag{B38}$$

$$C_{r\theta} = -\frac{15\text{Wi}}{4} \sin 2\theta [1 - \exp(-t)], \tag{B39}$$

$$C_{r\phi} = 0. \tag{B40}$$

The extensional stresslet can be evaluated by substituting this result into Eq. (B7) to calculate the traction, taking the integral of its moment as per Eq. (12), and calculating the extensional stresslet S_{ext} with the relevant components via Eq. (17), to give the following:

$$S_{\text{ext}}^{\text{poly}} = 4.5(1 - \beta)[1 - \exp(-t)]. \tag{B41}$$

[1] H. Lopez Hernandez, A. K. Grosskopf, L. M. Stapleton, G. Agmon, and E. A. Appel, Non-Newtonian polymer–nanoparticle hydrogels enhance cell viability during injection, Macromol. Biosci. **19**, 1800275 (2019).

[2] B. A. Aguado, W. Mulyasasmita, J. Su, K. J. Lampe, and S. C. Heilshorn, Improving viability of stem cells during syringe needle flow through the design of hydrogel cell carriers, Tissue Eng. Part A **18**, 806 (2012).

[3] D. Barthès-Biesel, Modeling the motion of capsules in flow, Curr. Opin. Colloid Interface Sci. **16**, 3 (2011).

[4] E. S. Shaqfeh and B. Khomami, The Oldroyd-B fluid in elastic instabilities, turbulence and particle suspensions, J. Non-Newton. Fluid Mech. **298**, 104672 (2021).

[5] D. L. Koch, E. F. Lee, and I. Mustafa, Stress in a dilute suspension of spheres in a dilute polymer solution subject to simple shear flow at finite deborah numbers, Phys. Rev. Fluids **1**, 013301 (2016).

[6] J. Einarsson, M. Yang, and E. S. G. Shaqfeh, Einstein viscosity with fluid elasticity, Phys. Rev. Fluids **3**, 013301 (2018).

[7] M. Yang and E. S. G. Shaqfeh, Mechanism of shear thickening in suspensions of rigid spheres in Boger fluids. Part I: Dilute suspensions, J. Rheol. **62**, 1363 (2018).

[8] R. Scirocco, J. Vermant, and J. Mewis, Shear thickening in filled boger fluids, J. Rheol. **49**, 551 (2005).

[9] S.-C. Dai, F. Qi, and R. I. Tanner, Viscometric functions of concentrated non-colloidal suspensions of spheres in a viscoelastic matrix, J. Rheol. **58**, 183 (2014).

[10] A. Jain, J. Einarsson, and E. S. G. Shaqfeh, Extensional rheology of a dilute particle-laden viscoelastic solution, Phys. Rev. Fluids **4**, 091301(R) (2019).
[11] A. Sharma and D. L. Koch, Steady-state extensional rheology of a dilute suspension of spheres in a dilute polymer solution, Phys. Rev. Fluids **8**, 033303 (2023).
[12] M. Yang, S. Krishnan, and E. S. Shaqfeh, Numerical simulations of the rheology of suspensions of rigid spheres at low volume fraction in a viscoelastic fluid under shear, J. Non-Newton. Fluid Mech. **233**, 181 (2016).
[13] G. Batchelor, The stress generated in a non-dilute suspension of elongated particles by pure straining motion, J. Fluid Mech. **46**, 813 (1971).
[14] A. Jain and E. S. G. Shaqfeh, Transient and steady shear rheology of particle-laden viscoelastic suspensions, J. Rheol. **65**, 1269 (2021).
[15] E. S. Shaqfeh, On the rheology of particle suspensions in viscoelastic fluids, AIChE J. **65**, e16575 (2019).
[16] M. Villone, F. Greco, M. Hulsen, and P. Maffettone, Simulations of an elastic particle in newtonian and viscoelastic fluids subjected to confined shear flow, J. Non-Newton. Fluid Mech. **210**, 47 (2014).
[17] C. J. Guido and E. S. Shaqfeh, The rheology of soft bodies suspended in the simple shear flow of a viscoelastic fluid, J. Non-Newton. Fluid Mech. **273**, 104183 (2019).
[18] A. Zhang and E. S. Shaqfeh, Rheology of non-brownian particle suspensions in viscoelastic solutions. part 1: Effect of the polymer concentration, J. Rheol. **67**, 499 (2023).
[19] E. Guazzelli and J. F. Morris, *A Physical Introduction to Suspension Dynamics* (Cambridge University Press, Cambridge, UK, 2011), Vol. 45.
[20] F. A. Morrison, *Understanding Rheology*, Raymond F. Boyer Library Collection (Oxford University Press, New York, 2001).
[21] F. Ham, K. Mattsson, and G. Iaccarino, Accurate and stable finite volume operators for unstructured flow solvers, Center for Turbulence Research Annual Research Briefs, 243 (2006).
[22] S. Krishnan, E. S. Shaqfeh, and G. Iaccarino, Fully resolved viscoelastic particulate simulations using unstructured grids, J. Comput. Phys. **338**, 313 (2017).
[23] D. L. Koch and G. Subramanian, The stress in a dilute suspension of spheres suspended in a second-order fluid subject to a linear velocity field, J. Non-Newton. Fluid Mech. **138**, 87 (2006).
[24] A. Saadat, C. J. Guido, G. Iaccarino, and E. S. G. Shaqfeh, Immersed-finite-element method for deformable particle suspensions in viscous and viscoelastic media, Phys. Rev. E **98**, 063316 (2018).
[25] K. D. Housiadas and R. I. Tanner, On the rheology of a dilute suspension of rigid spheres in a weakly viscoelastic matrix fluid, J. Non-Newton. Fluid Mech. **162**, 88 (2009).
[26] F. Greco, G. D'Avino, and P. Maffettone, Rheology of a dilute suspension of rigid spheres in a second order fluid, J. Non-Newton. Fluid Mech. **147**, 1 (2007).